Processing and Application of Ceramics 19 [4] (2025) 380–388
https://doi.org/10.2298/PAC2504380G

Influence of alumina particle size on the properties of crucibles utilised in thermogravimetry

Magdalena Gromada*

Institute of Power Engineering – National Research Institute, 01-330 Warsaw, Mory 8, Ceramic Division CEREL, 36-040 Boguchwała, Techniczna 1, Poland

Received 2 October 2025; Received in revised form 27 November 2025; Accepted 9 December 2025

Abstract

Crucibles for thermogravimetric analysis utilised in a derivatograph must meet demanding requirements regarding the material and accuracy of shape, dimensions and weight. The material for crucibles must demonstrate a high operating temperature and resistance to thermal shock, chemical inertness and excellent thermal conductivity. The influence of the four different alumina powders, having bimodal size distribution with different sizes of the fine and coarse particles, on important performances of DTA/DTG crucibles fabricated via the high-pressure injection moulding method was investigated. In addition, the influence of different amount of thermoplasticiser was investigated too. The sintered sample prepared with the finest alumina powder has optimal performances, i.e. high apparent density of 3.93 g/cm^3, mechanical strength of 383 MPa, high hardness of 13.75 GPa, fracture toughness of 5.04 MPa·m$^{0.5}$, relatively small coefficient of thermal expansion of 7.61 × 10^{-6} 1/K, and low material surface roughness of 0.23 μm. Crucibles fabricated with this precursor revealed high functional properties and met rigorous quality requirements.

Keywords: *alumina crucibles, high-pressure injection moulding, structure, mechanical properties*

I. Introduction

Thermogravimetry is an analytical method that involves subjecting a sample to controlled heating in a specific atmosphere, tracking the associated mass changes with the use of a microbalance and recording the mass change data as a function of temperature or time controlled by computer software [1]. This method is mainly applied for the characterisation and investigation of structural decomposition, thermal stability and phase transitions [2]. Thermogravimetric analysis is widely utilised in industrial laboratories for the assessment of diverse materials, e.g. precursor materials [3], carbonates [4], polymers [5], biomass [6], coal [7], liquid fuels [8], catalysts [9] and soil [10]. Thermogravimetric analysis (TGA) is often used in studies of the thermal decomposition of biomass, such as the pyrolysis of substances in diverse conditions and heating rates. Differential thermal gravimetric thermograms can be used to determine the reaction rates and time constants of the diverse steps of thermal treatment [11]. Chong *et al.* [12] investigated the pyrolysis of some organic substances and wastes, such as manures, whereas Xu *et al.* [13] studied the decomposition of microalgae. Yap and Losic [14] utilised thermogravimetric analysis for the characterisation and quality control of raw materials, supporting materials and electrodes to develop emerging energy storage devices.

Crucibles for thermogravimetric analysis on a derivatograph, owing to the specificity of the analysis performed with their utilisation, must meet high requirements regarding the material from which they are made and the accuracy of shape, dimensions and weight [15]. The material for crucibles must demonstrate a high maximum working temperature and resistance to thermal shock, chemical inertness and excellent thermal conductivity. Crucible has the diameter of only 6.90 mm, the wall thickness of 0.45 mm and the weight of 0.210 g, where the acceptable deviation of the crucible weight can be within the range of ±0.001 g. The quality control of crucibles for DTA/DTG analysis requires checking cracks with the use of a dye penetrant, examining the shape and dimensions (diameter, height, wall thickness), and inspecting the weight of each crucible.

*Corresponding author: +48 504 745 364
e-mail: *magdalena.gromada@cerel.pl*

Considering the requirements for crucibles, the high-pressure injection moulding, one of the promising moulding methods, was applied. This processing technique allows the formation of sophisticated elements with relatively small cross-sections and a shape that precisely reproduces the finished product. The high-pressure injection moulding method ensures a fast production and a low cost of product manufacturing; however, owing to the high cost of the mould preparation, it is used in series production. This method, which uses high pressure during the shaping of products, eliminates the formation of large pores that often appear when low- or medium-pressure injection is used [16,17]. The high-pressure injection moulding method requires the development of a powder with an appropriate particle size distribution, the selection of a thermoplasticiser, parameters for feedstock preparation, determination of the optimal parameters of high-pressure injection, conditions for removing the thermoplasticiser and final sintering [18–22].

In injection moulding method, the powder processing plays important role. To enable the correlation of powder behaviour at each processing step, a powder must be characterised for the initial physical features (size, distribution, shape). The content of powder, which is included in continuous binder matrix to obtain high green density and dimension accuracy of products after sintering, depend on its packing characteristics. Moreover, the particle packing method has significant impact on the rheology of the feedstocks. Particle shape strongly influences different packing characteristics while the highest packing density, defined as the ratio of solid particle volume to total volume, is obtained with the use of round particles. Mechanical activation of powders reduces any roughness on the surface of particles resulting in round particles and as a result higher packing density. The uniform particle size distribution ensures obtaining the higher packing density as the finer particles fill the spaces between the large ones. Two possible methods to broaden the particle size distribution can be applied: combination of mixture of two or more particle classes or a selection of wide continuous distribution of particle size [17,21,23].

The alumina feedstock preparation for the injection moulding method is still under research. Wei *et al.* [24] investigated the pressure-volume-temperature curve of feedstock mixed with submicron alumina powder. They measured the properties of injected moulded pieces, including the moulded mass, green density and dimensional change of the green pieces, apparent density and fracture toughness of the sintered samples. Liu *et al.* [25] studied the effects of binder composition on the thermal behaviour and mechanical properties of a ceramic injection moulded system. To produce transparent alumina pieces, Estarki *et al.* [26] dispersed alpha-alumina nanoparticles with different amounts of MgO, used as a sintering aid, in a paraffin-polypropylene-based binder system. They optimised alumina-binder feedstock for the injection moulding method. After binder removal, the green body piece was sintered via the spark plasma sintering method. They determined the feed fluidity, hardness, flexural strength and density of the sintered pieces. Masihi *et al.* [27] optimised a feedstock containing alumina-binder nanoparticles for ceramic injection moulding to create translucent alumina parts. The results showed that a combination of ceramic injection moulding and spark plasma sintering (SPS) methods caused more visible transmission than the conventional SPS of alumina nanopowder. The wear rate of the as-obtained transparent sample was proportional to the alumina grain size.

The aim of this work is to investigate the influence of the powder particle size distribution on the properties of feedstock processing (injection temperature, speed and pressure and cavity filling quality), which affect the performances of the material and the crucibles after sintering (density, bending strength, hardness, fracture toughness, thermal expansion coefficient and surface roughness).

II. Experimental

2.1. Powders and feedstocks

To satisfy the high requirements for the crucible material, four different alumina powders were selected: alumina 626-31 (Nabaltec), 713-10 (Nabaltec), mixture of 626-31 and 713-10 powders (mass ratio 1 : 1) and A16 SG (Almatis). The powders have different particle sizes and are denoted as LF-LC SF-SC, LF-SC and SF-LC, respectively.

The total content of Na_2O for both alumina 626-31 and 713-10 was 0.1 wt.%, while for the powder A16 SG it was 0.07 wt.%. Moreover, the alumina 713-10 and A16 SG contain 0.08 wt.% and 0.05 wt.% of MgO, respectively. These sintering additives in such small amount improve sinterability of alumina powders without causing the grains growth. The particle size distributions of the selected powders were determined via laser diffraction on a Mastersizer 2000 granulometer (Malvern). Reflective index (*RI*) was equal to 1.765, absorption was 0.01 and General particle size model was applied during measurement. The pore size distribution and pore volume of the alumina powders were determined with an AUTOPORE 4 9500 (Micromeritics) via the mercury porosimetry method with maximum pressure of 228 MPa.

In the next step, different feedstocks (Table 1) were prepared with the use of a TP 6000 thermoplasticiser (Zschimmer & Schwarz) and stearic acid (Chempur) which works as a dispersant agent. The TP 6000 thermoplasticiser was melted in a GC-MIX-12/13 mixer (Goceram AB) at 130 °C; after that, stearic acid and alumina powders preheated at 130 °C were added. The homogenisation process was performed at 130 °C for 1 h.

DTA/DTG analysis of the thermoplasticiser TP 6000 was performed in air on the STA 449 F5 Jupiter

Table 1. Composition of feedstocks with the use of a TP 6000 thermoplasticiser and stearic acid, as well as some important parameters of injection process

Feedstock	625-31 [wt.%]	713-10 [wt.%]	A16 SG [wt.%]	Stearic acid [wt.%]	TP 6000 [wt.%]	Nozzle/mould temperatures	Injection pressure / injection speed
LF-LC-13	86.0			1.0	13.0	81 °C/ 41 °C	1200 bar / 11.7 cm^3/s
LF-LC-12	87.0			1.0	12.0	81 °C/ 41 °C	1200 bar / 11.7 cm^3/s
SF-SC-13		86.0		1.0	13.0	87 °C/ 45 °C	1200 bar / 11.4 cm^3/s
SF-SC-14		85.0		1.0	14.0	87 °C/ 43 °C	1200 bar / 11.4 cm^3/s
LF-SC-13	43.0	43.0		1.0	13.0	87 °C/ 43 °C	1200 bar / 11.4 cm^3/s
LF-SC-14	42.5	42.5		1.0	14.0	87 °C/ 43 °C	1200 bar / 11.4 cm^3/s
SF-LC-13			86.0	1.0	13.0	91 °C/ 45 °C	1400 bar / 10.7 cm^3/s
SF-LC-12			87.0	1.0	12.0	91 °C/ 45 °C	1400 bar / 10.7 cm^3/s

derivatograph (Netzsch). The sample of 21.83 mg weight was heated with the rate of 1 °C/min to the maximal temperature of 600 °C. The rheological properties of the alumina feedstocks were investigated by using a rotational rheometer Kinexus Pro (Malvern Instruments) equipped with a thermostatic unit. The tests were performed at 100 °C by using parallel plates with rotor diameter of 60 mm and fixing 0.500 mm of gap between the plates. Flow curves in controlled rate mode between 0.1 and 10^4 s^{-1}, by considering 11 points in logarithmic scale with a time per point of 60 s, were obtained to determine the dependency of shear viscosity on shear rate. The flow index (n) and the consistency index (k) with the correlation coefficient at least 0.99 were extracted by applying the Ostwald-de Waele's model.

2.2. Shaping and sintering

The test pieces (with a diameter of 6 mm and a length of 60 mm) were prepared with a two-cavity mould. After sintering, these test pieces were used to determine the apparent density, open porosity, water absorbability, bending strength, hardness, fracture toughness, thermal expansion coefficient and surface roughness. The selection of injection parameters included many variables concerning temperature, pressure, speed, volume and time. The incorrect setting of even one parameter resulted in the appearance of defects in the moulded parts.

The injection process was carried out on a BOY XS high-pressure injection moulding machine (BOY Machines) with a mould clamping force of 100 kN, a maximum injection volume of 6.1 cm^3 and a maximum injection pressure of 230 MPa. The optimal injection parameters for all materials in the process of the test piece formation included a plasticising speed of 80 mm/s, a clamping pressure of 525 bar with a clamping time of 1 s, an injection volume of 5.65 cm^3, a mould clamping force of 100 kN and a dwell time of 40 s. Different temperatures of the nozzle in each zone and mould temperature were used (Table 1). The same injection pressure of 1100 bar was applied in the last zone, but different pressures were used in the initial zone (Table 1). The injection speeds were 11.4 and 11.7 cm^3/s depending on the feedstock (Table 1).

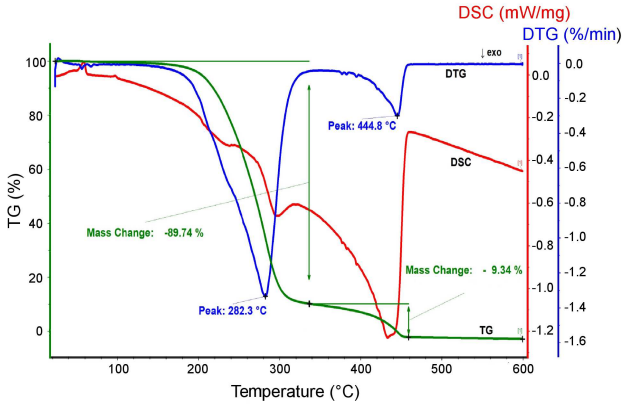

Figure 1. DTA/DTG analysis of thermoplasticiser TP 6000

In the process of debinding and sintering of the materials, an electric furnace FCF 117/170 M (Czylok) equipped with fans for blowing heated air and removing it from the furnace chamber was used. DTA/DTG analysis was used to design the heating speed and dwell time for the thermal removal of thermoplasticiser TP 6000 from test pieces and crucibles. According to the TG curve of the TP 6000 thermoplasticiser (Fig. 1), there is no mass loss at temperatures below 160 °C. However, a rapid loss of mass reaching 89.74%, slight mass loss of 9.34% and a very slight loss of 0.92% were observed in temperature intervals 160–340 °C, 340–450 °C and 450–600 °C, respectively. On the basis of the DTA/DTG analysis, the thermal removal of the thermoplasticiser TP 6000 from the test pieces was performed at 450 °C for 2 h. The heating rate was 12 °C/h, and the samples were allowed to cool freely in the furnace. The final sintering of the test pieces was completed at 1620 °C with a dwell time of 1.5 h. The heating rate to the maximum temperature was set as 100 °C/h, while the cooling rate was equal to 200 °C/h to a temperature of 600 °C, below that free cooling in a furnace was applied.

2.3. Processing of alumina crucibles

The alumina crucibles were manufactured from the selected material with the optimal performance by using BOY XS injection moulding machine (BOY Machines) and specially designed mould, enabling the formation of thin-walled crucibles. In the process of forming of crucibles for thermogravimetric analysis, a single-cavity

mould was used. The feedstock was fed to the mould cavity by two opposite sides of the cylindrical surface at the ends of the element wall. This solution allowed the correct filling of the wall and bottom of the DTA/DTG crucibles, which were only 0.45 mm thick. The injected streams of material join in the middle of the crucible bottom, which can cause cracks or empty spaces with air. To prevent the crucibles from being damaged when being pulled out of the mould, an ejector in the form of the entire bottom surface was applied. During the injection process, a set of optimal injection parameters was developed to protect the moulded goods from defects and deformation. The temperature of the cylinder and the nozzle was 87 °C, with a tolerance of 2 °C. The injection pressure was equal to 1200 bar in the initial zone and 1100 bar in the last zone, while the velocity of injection was equal to 19.3 cm^3/s. The temperature of the mould was held at 44.4 °C, and the time for which the crucibles remained in the mould was 42 s. Debinding and sintering of the alumina crucibles was performed under the same conditions as those used for the test pieces.

2.4. Characterization

The apparent density, open porosity and apparent absorbability of the sintered test pieces were determined via Archimedes' principle and the boiling method to saturate them with water. The hardness and fracture toughness (K_{IC}) were measured via a 430/450SVD Vickers hardness tester (Wilson Hardness). The test pieces were first embedded in acrylic resin and then ground on #500 and #1200 diamond discs. The final pre-processing was performed via a polishing cloth with a diamond suspension with a grain size equal to 3 and 1 µm. The coefficient of thermal expansion at 600 °C was determined via the L75 high-temperature dilatometer (Linseis Messgeräte GmbH). The bending strength of the materials was determined according to standard PN-EN 60672-2:2002 via the three-point method on sintered beams with a ZDM-5 strength testing machine (VEB). The surface roughness was measured with a MarSurf PS 10 profilometer (Mahr Inc.). For the purpose of microstructural analysis, the ground and polished cross-section of a crucible was additionally thermally etched at 1500 °C for 2 h. The microstructure was examined using a scanning electron microscope (SEM, HITACHI S-3400N/2007).

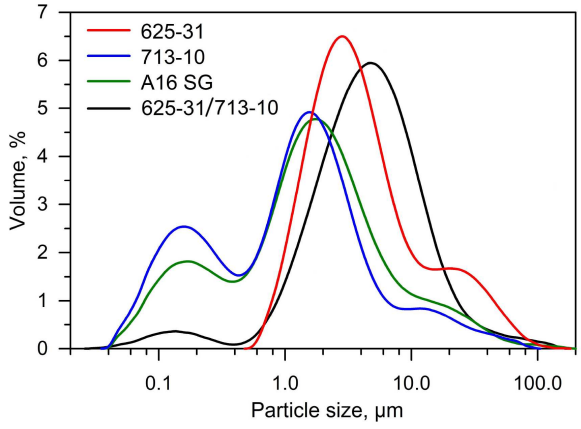

Figure 2. The particle size distribution of alumina powders

III. Results and discussion

3.1. Characterization of alumina powders

Figure 2 shows that all the alumina powders are characterised with very wide particle size distributions ranging from 0.035 to 120 µm, which should ensure the high densification of materials after sintering [17]. The median particle size (d_{50}), the fine particle threshold (d_{10}) and the coarse particle threshold (d_{90}), determined directly from the cumulative particle size distribution, are given in Table 2.

The powders are characterized with broad particle size distributions and the presence of evident peaks in the range of fine and coarse particles. The finest powders were 713-10 and A16SG, and the coarsest were 625-31 and 625-31/713-10 mixture. In addition, the powders have different distributions in the range of fine (F) and coarse (C) particles. According to these differences they are denoted as SF-SC, SF-LC, LF-SC and LF-LC, where S and L stay for small and large sizes, respectively (Table 2).

The observed broad particle size distributions of alumina powders with the presence of evident peaks in the range of fine and coarse particles should ensure obtaining the higher packing density of shaped pieces in injection moulding process as the finer particles fill the holes between the large ones [17,21]. The obtaining of high density of the shaped pieces directly influences the density of sintered materials which in turn should ensure the high mechanical properties, hardness and fracture toughness.

The differential cumulative pore volume curves of the alumina powders, presented in Fig. 3a, indicate two populations of pores. The first peak, situated in the region of pore size diameter ranging from 10 to 100 µm,

Table 2. Median particle size (d_{50}), fine particle threshold (d_{10}) and coarse particle threshold (d_{90}) determined directly from the particle size distribution as well as median pore diameter (D_m) and cumulative pore volume (D_C)

Sample	Powder	d_{10} [µm]	d_{50} [µm]	d_{90} [µm]	D_m [µm]	D_C [mm^3/g]
LF-LC	625-31	1.2	3.3	20.7	2.22	496.4
SF-SC	713-10	0.1	1.1	6.1	1.28	679.4
LF-SC	625-31/713-10	1.2	4.2	13.5	1.06	579.3
SF-LC	A16 SG	0.1	1.5	8.7	6.23	576.4

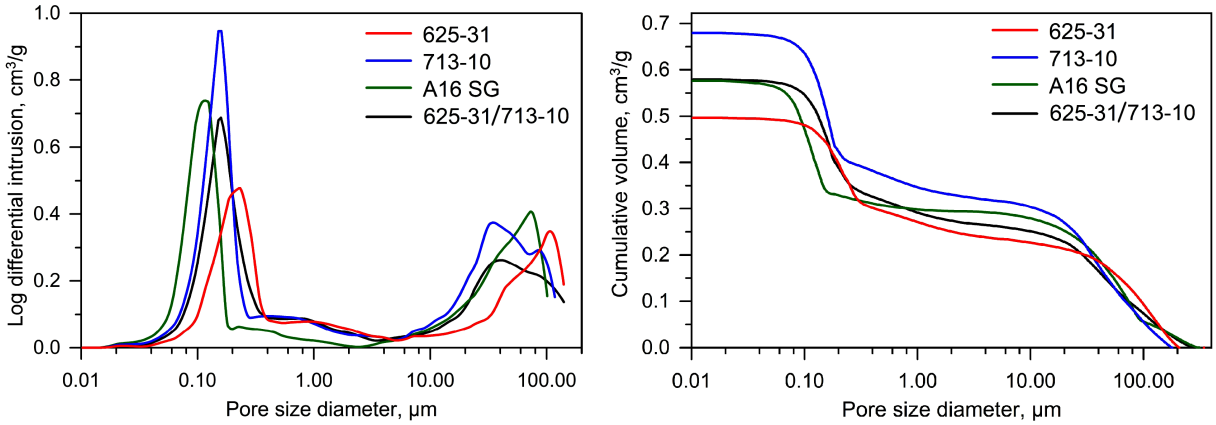

Figure 3. Differential (a) and cumulative pore volume (b) as a function of the pore size diameter for alumina powders

concerns inter-particle pores, while the second one occurring in the range of small pores (0.09 to 0.16 μm) presents pore volume within particles. The maximum value of cumulative pore volume shown in Fig. 3b and indicated in Table 2 gives the apparent specific pore volume, in the meso- and macropore range because it includes inter-particle porosity of the material, intra-particle porosity of the sample, and any volumetric change of the sample resulting from pressurization. The cumulative pore volume ranges from 496.4 mm^3/g for the powder 625-31 (SF-LC) to 679.4 mm^3/g for the alumina 713-10 (SF-SC). Moreover, Table 2 contains results of median pore diameter, which is the most representative parameter of pore size in the whole range of pores distribution as it takes into account both inter-particle voids and pores volume within particles. The smallest value of median pore diameter was obtained for the 713-10 and 625-31/713-10 alumina powders (Table 2). However, the highest median pore diameter equal to 6.23 μm was obtained for the powder A16 SG (SF-LC). The obtained values of median pore diameter and cumulative pore volume of alumina powders will ensure the high efficiency process of feedstocks preparation. As a result of presence of small pores, each alumina particle can be freely surrounded by the thermoplasticiser, which in turn positively influences the rheological properties of feedstocks and injection parameters choice as well as obtaining high level of densification in the shaping process.

3.2. *Characterization of alumina feedstocks*

The flow curves indicated in Fig. 4 point that all the alumina materials used for injection behave as typical pseudoplastic fluids, i.e. they show shear-thinning, for which the apparent viscosity decreases with an increasing shear rate. Behaviour of the flow curves can be fitted by the Ostwald-de Waele's model described approximately by a power-law ($\eta = k\gamma^{n-1}$) from which the power law constant (n) and the consistency index (k) were obtained.

The lowest values of consistency index k were obtained for the feedstocks LF-LC-13 and LF-LC-12 originated from the powder with coarse particles, where decreasing of thermoplasticiser content by 1 wt.% caused increase of the viscosity and decrease of the shear-thinning properties (Table 3). The same tendency is visible in the case of the feedstock SF-SC-13 and SF-SC-14 originated from the finest powder 713-10 (Table 3). The opposite tendency is visible in the case of the feedstocks LF-SC-13 and LF-SC-14 originated from the A16 SG powder which have the highest index k and flow index n (Table 3).

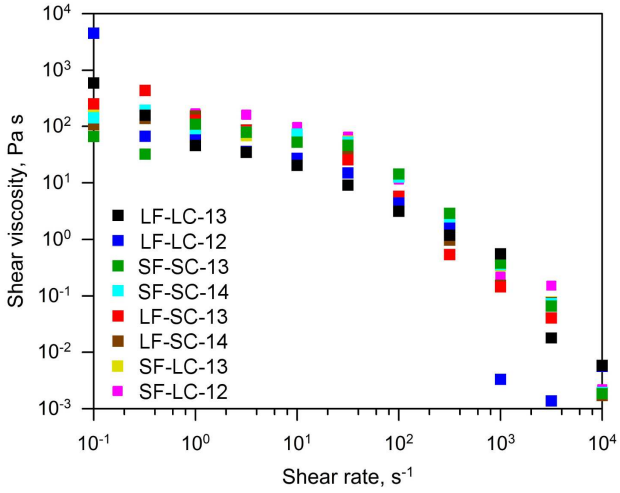

Figure 4. Flow curves for alumina feedstocks

The shear viscosity for all materials ranges from 10^{-1} to 10^2 s^{-1} revealing almost linear relationship, but considerable reduction is obvious for shear rate above 10^2 s^{-1}. Differences between shear viscosity values for different materials are the highest at small shear rates.

The injection parameters are independent of the thermoplasticiser volume, but the nozzle and mould temperature, pressure and injection speed are related to the particle size distribution of the alumina powders, as shown in Table 1.

The test pieces shaped by injection moulding with different alumina powder particle size and the same quantity of 13 wt.% thermoplasticiser revealed very

Table 3. The power law constant (n) and the consistency index (k) of the prepared feedstocks

Feedstock	Powder	k [Pa·s]	n
LF-LC-13	625-31	45.7	0.24
LF-LC-12		57.2	0.33
SF-SC-13	713-10	109.3	0.46
SF-SC-14		89.3	0.24
LF-SC-13	mixture	128.5	0.15
LF-SC-14		152.3	0.16
SF-LC-13	A16 SG	137.2	0.47
SF-LC-12		169.8	0.63

similar values of apparent green density. However, dependence between an apparent density and the particle size of the powder is visible and grows with decreasing particle size. Thus, the lowest apparent density equal to 2.70 g/cm^3 was obtained for the LF-LC-13 sample originated from the powder with coarse particles, while the highest apparent density equal to 2.73 g/cm^3 was obtained for the SF-SC-13 sample made of the fine-grained alumina powder.

3.3. Characterization of sintered samples

According to standard EN 60672-3 [28], high-alumina ceramics C799 should have an apparent density of at least 3.7 g/cm^3, open porosity of 0.0%, bending strength of at least MPa and coefficient of thermal expansion 7–8 $\times 10^{-6}$ 1/K. The properties of the sintered materials are presented in Table 4.

In the case of the LF-LC-13 and LF-LC-12 materials, which originated from the coarsest alumina 626-31 powder, the apparent density, open porosity and bending strength do not satisfy the standard EN 60672-3 (Table 4). Further improvements in material properties will necessitate the application of higher sintering temperatures, but such solution does not possess any economic justification.

For the material SF-LC-12, derived from the alumina A16 SG powder with fine particles, but large inter-particle pores (Fig. 2) and the smallest volume of thermoplasticiser (12.0 wt.%), higher apparent density was achieved. However, such improvement did not involve an appropriate level of mechanical strength. However, increasing the termoplasticiser content for 1 wt.% in feedstock SF-LC-13 significantly improved the bending strength, hardness and fracture toughness which satisfied the requirements of the standard EN 60672-3.

The materials SF-SC-13 and SF-SC-14 have the best parameters after sintering and were produced from the alumina 713-10, which is the finest powder having the smallest inter-particle pores (Fig. 2). These materials are characterised by very high apparent densities ranging from 3.89 to 3.93 g/cm^3, as well as the highest bending strength in the range of 375–383 MPa, very high hardness values over 13.75 GPa and fracture toughness values greater than 4.77 MPa·m$^{0.5}$.

The materials LF-SC-13 and LF-SC-14, fabricated from mixed 625-31/713-10 powder, which have smaller portion of fine particles and higher portion of large particles, also exhibited good properties. Small particles filled in gaps between coarser ones, and as a result, the compaction of green bodies was high. Therefore, the apparent density of these materials after sintering was high, but the bending strength is somewhat lower than in the case of the SF-SC-13 and SF-SC-14 samples. However, their performances are good and in the range of standard EN 60672-3.

The value of apparent density of the sintered test pieces, originated from different alumina powders with the same quantity of thermoplasticiser (13 wt.%), increases together with decreasing the alumina particle size. The lowest value of apparent density equal to 3.71 g/cm^3 has the material LF-LC-13 obtained from the alumina powder with coarse particles and the largest inter-particle pores. The density rises to 3.86 g/cm^3 for the material LF-SC-13 and finally increases to 3.89 and 3.90 g/cm^3 for the materials SF-SC-13 and SF-LC-13 (prepared from the alumina powder with finer alumina particles), respectively.

It should be underlined that the surface roughness of shaped pieces is mainly affected by the quality of mould cavities, which were polished to R_a value of 0.16 µm. However, the surface roughness of the sintered alumina test pieces is also influenced by the particle size distribution of the used powders. In the process of forming by high pressure injection moulding method, segrega-

Table 4. Properties of all prepared test pieces

Material	Water absorbability [%]	Apparent density [g/cm^3]	Open porosity [%]	Bending strength [MPa]	Hardness HV [GPa]	Fracture toughness [MPa·m$^{0.5}$]	Coefficient of thermal expansion [1/K]	Surface roughness [µm]
LF-LC-13	1.18	3.71	4.36	241	-	-	7.57×10^{-6}	0.21
LF-LC-12	1.43	3.65	5.21	246	-	-	7.62×10^{-6}	0.21
SF-SC-13	0.01	3.89	0.03	375	13.92	4.77	7.65×10^{-6}	0.37
SF-SC-14	0.01	3.93	0.03	383	13.75	5.04	7.61×10^{-6}	0.23
LF-SC-13	0.03	3.86	0.11	313	13.54	4.79	7.63×10^{-6}	0.43
LF-SC-14	0.03	3.90	0.10	310	13.99	4.83	7.64×10^{-6}	0.42
SF-LC-13	0.01	3.90	0.04	312	11.71	5.09	7.70×10^{-6}	0.30
SF-LC-12	0.01	3.94	0.04	187	-	-	7.68×10^{-6}	0.38

tion of coarse and fine particles can lead to differences in surface roughness. Thus, during injection moulding of the alumina powder with coarse particles (LF-CS), the larger particles were collected near the boundary of mould cavity and the surface roughness of the materials LF-SC-13 and LF-SC-14 is the highest and depends little on the thermoplasticiser amount. On the other hand, the surface roughness of the materials SF-SC-13 and SF-SC-14, fabricated by using the alumina powder with fine particles is significantly lower. In addition, the higher thermoplasticizer content caused decrease of surface roughness meaningfully, which was connected with the better surrounding of particles and as a result the enhanced their compaction. To summarise, the lower particle size of precursor powder and higher thermoplasticiser content caused the smallest surface roughness.

The bending strength of alumina after sintering is influenced by a critical flaw in the material, which is commonly proportional to the size of the grains. Therefore, the mechanical strength is high when the sintered alumina is dense and the microstructure is fine and homogeneous, due to a reduction in flaw size [29,30]. The size of grains in sintered materials is directly related to the particle size distribution of starting alumina powder. This trend is also clearly visible for the sintered test samples and the highest bending strength has material originated from the finest alumina powder, i.e. SF-SC. The value of hardness is also mainly influenced by the grain size of sintered materials and it increases together with decreasing of grain size [31,32]. For the fine-grained materials, the fracture toughness is generally low and it increases when large elongated or plate-like grains are randomly dispersed in a fine-grained matrix. During the fracture process, these large grains resist crack propagation effectively [33].

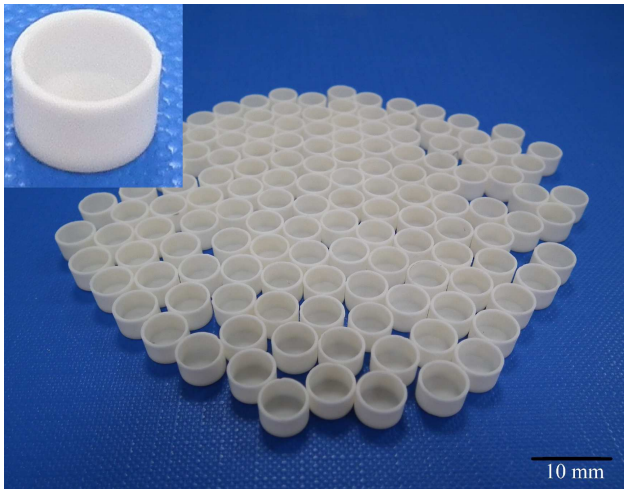

Figure 5. Alumina crucibles for thermogravimetric analysis fabricated from material SF-SC-14

3.4. Crucible performances

On the basis of the results presented in Table 4, the material SF-SC-14, which has the most favourable properties (Table 4), was selected because it meets all the requirements for crucibles utilised in thermogravimetric analysis. The apparent density and mechanical strength of the material SF-SC-14 have very compatible values to results achieved by Wei *et al.* [24]. The value of fracture toughness is 26% higher than presented by Xu *et al.* [34] and even 36% higher than reported by Riu *et al.* [33]. However, the value of hardness is 16% lower than presented by Riu *et al.* [33]. Moreover, the value of the coefficient of thermal expansion was on the same level as in paper published by Kuscer *et al.* [35].

Figure 5 shows alumina crucibles after sintering, which were checked for the presence of cracks via a dye penetrant (Diffu-Therm), and a visual inspection of the crucibles was carried out for the presence of closed pores. Owing to the use of optimal injection parameters, the crucibles did not present any defects.

Figure 6a presents dense homogenous microstructure of a crucible cross-section. The size of grains ranges from 2 to even 20 μm and grain boundaries are softly bordered. In the corners of grains, a small pore of the size less than 1 μm is visible, which confirms result of an open porosity of the material SF-SC-14 equal to 0.03% included in Table 4. Figure 6b with higher magnification

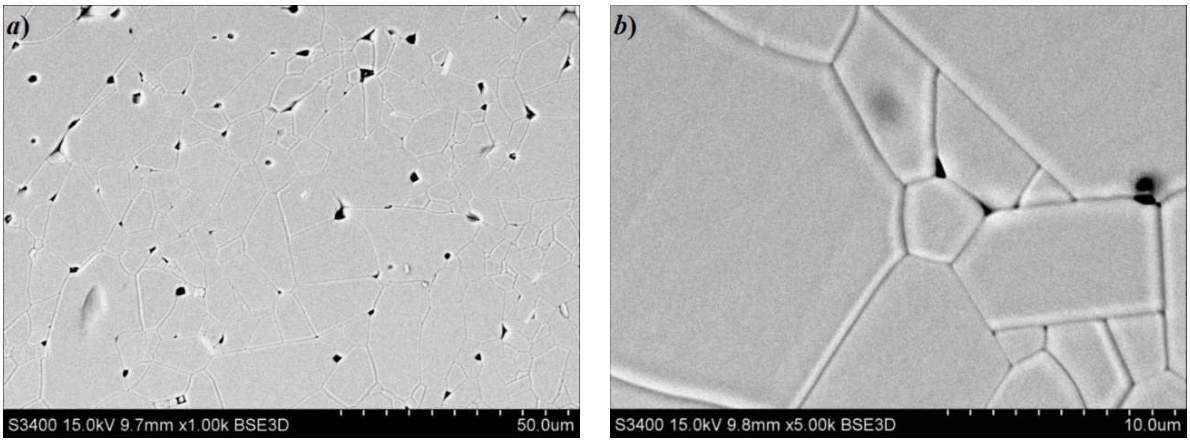

Figure 6. Cross-section SEM microstructure of crucible fabricated from material SF-SC-14 in magnification of 1000× (a) and 5000× (b)

shows well packed grains various sizes with the presence of sporadic small pores in the corners of grains.

In addition, a quality acceptance of crucibles for DTA/DTG analysis was carried out, which included control of the shape and dimensions (diameter, height, wall thickness) as well as the weight of each crucible. The diameter of the crucible is only 6.90 mm, and the wall thickness is 0.45 mm. These dimensions were maintained for the entire batch of 200 crucibles with an accuracy of ±0.01 mm. The weight of the crucible was 0.210 g, and the weight deviation of the crucible mass was within the range of ±0.001 g. Therefore, the obtained crucibles for thermogravimetric analysis revealed very good material parameters as well as shape and dimension repeatability, which allowed the use of these crucibles in domestic analyses.

IV. Conclusions

The influence of the four different alumina powders, having bimodal size distribution with different sizes of the fine and coarse particles, on important properties of DTA/DTG crucibles fabricated via the high-pressure injection moulding method was investigated. In addition, the influence of different amount of thermoplasticiser was investigated too. It was shown that the optimal alumina powder for crucible fabrication was characterised by the smallest particle size, narrowest particle size distribution (the smallest average particle size of 1.1 μm, the smallest d_{10} of 0.1 μm and d_{90} not exceeding 6.1 μm) and smallest inter-particle pores. Moreover, the feedstock (obtained from the selected optimal alumina powder) has the medium values of consistency index k equal to 89.3 Pa·s and flow index n reaching 0.24. The injection process required to apply an average nozzle and mould temperatures at typical injection pressures and speeds. The optimal alumina material containing 14 wt.% of thermoplasticiser TP 6000 after sintering reveals higher apparent density and bending strength, much higher fracture toughness, slightly lower hardness and thermal expansion coefficient, and lower surface roughness than material containing 13 wt.% of thermoplasticiser.

Acknowledgement: This work was financed by funds for statutory activities No. OC/02/STAT/2024 realised by Institute of Power Engineering – National Research Institute Ceramic Division CEREL.

References

1. D. Losic, F. Farivar, P.L. Yap, "Refining and validating thermogravimetric analysis (TGA) for robust characterisation and quality assurance of graphene-related two-dimensional materials (GR2Ms)", *C*, **10** [2] (2024) 30.
2. S.S. Stino, "Thermal analysis of dental materials", *Biomater. J.*, **1** [12] (2022) 15–23.
3. P.B. Arab, T.P. Araújo, O.J. Pejon, "Identification of clay minerals in mixtures subjected to differential thermal and thermogravimetry analyses and methylene blue adsorption tests", *Appl. Clay Sci.*, **114** (2015) 133–140.
4. I. Galan, F. P. Glasser, C. Andrade, "Calcium carbonate decomposition", *J. Therm. Anal. Calorim.*, **111** (2013) 1197–1202.
5. X. Zhang, M. Han, L. Xu, A.M. AlSofi, "Long-term stability prediction of polyacrylamide-type polymers at harsh conditions via thermogravimetric analysis", *Chem. Phys. Lett.*, **795** (2022) 139538.
6. J.F. Saldarriaga, R. Aguado, A. Pablos, M. Amutio, M. Olazar, J. Bilbao, "Fast characterization of biomass fuels by thermogravimetric analysis (TGA)", *Fuel*, **140** (2015) 744–751.
7. A. Hassid, M. Klinger, S. Krzack, H. Cohen, "TGA-DSC combined coal analysis as a tool for QC (quality control) and reactivity patterns of coals", *ACS Omega*, **7** (2022) 1893–1907.
8. T. Vega-Lizama, L. Díaz-Ballote, E. Hernández-Mézquita, F. May-Crespo, P. Castro-Borges, A. Castillo-Atoche, G.G. González-García, L. Maldonado, "Thermogravimetric analysis as a rapid and simple method to determine the degradation degree of soy biodiesel", *Fuel*, **156** (2015) 158–162.
9. G.F. Leal, L.A. Ramos, D.H. Barrett, A.A.S. Curvelo, C.B. Rodella, "A thermogravimetric analysis (TGA) method to determine the catalytic conversion of cellulose from carbon-supported hydrogenolysis process", *Thermochim. Acta*, **616** (2015) 9–13.
10. M. Kristl, M. Mursec, V. Sustar, J. Kristl, "Application of thermogravimetric analysis for the evaluation of organic and inorganic carbon contents in agricultural soils", *J. Therm. Anal. Calorim.*, **123** (2016) 2139–2147.
11. C. De Blasio, "Thermogravimetric analysis (TGA)" in: *Fundamentals of Biofuels Engineering and Technology. Green Energy and Technology*. Springer, Cham, 2019.
12. C.T. Chong, G.R. Mong, J.-H. Ng, W.W.F. Chong, F.N. Ani, S.S. Lam, H.C. Ong, "Pyrolysis characteristics and kinetic studies of horse manure using thermogravimetric analysis", *Energy Convers. Manage.*, **180** (2019) 1260–1267.
13. Q. Xu, C. Ling, J. Li, "Microalgae decomposition in CO_2 atmospheres by thermogravimetric analysis", *Energy Procedia*, **123** (2019) 381–386.
14. P.L. Yap, D. Losic, "Methods and instruments thermal analysis", pp. 263–280 in: *Encyclopedia of Electrochemical Power Sources (Second Edition)*, Ed. J. Garche, Elsevier, 2025.
15. D. Furniss, A.B. Seddon, "Thermal analysis of inorganic compound glasses and glass-ceramics", in *Principles and Applications of Thermal Analysis*. Blackwell Publishing Ltd, 2008.
16. M. Gromada, A. Tłuczek, R. Cygan, "Silica-based ceramic cores for high-pressure turbine airfoil blades in aircraft engines", *Process. Appl. Ceram.*, **18** [3] (2024) 299–306.
17. B.C. Mutsuddy, R.G. Ford, *Ceramic Injection Molding*, Springer-Verlag, USA, 1994.
18. F. Hu, W. Liu, Z. Xie, "Surface modification of alumina powder particles through stearic acid for the fabrication of translucent alumina ceramics by injection molding", *Ceram. Int.*, **42** (2016) 16274–16280.
19. W. Liu, Z. Xie, T. Bo, X. Yang, "Injection molding of surface modified powders with high solid loadings: A case for fabrication of translucent alumina ceramics", *J. Eur. Ceram. Soc.*, **31** (2011) 1611–1617.
20. A. Mannschatz, S. Höhn, T. Moritz, "Powder-binder sep-

aration in injection moulded green parts", *J. Eur. Ceram. Soc.*, **30** (2010) 2827–2832.
21. A. Mannschatz, A. Müller, T. Moritz, "Influence of powder morphology on properties of ceramic injection moulding feedstocks", *J. Eur. Ceram. Soc.*, **31** (2011) 2551–2558.
22. P. Thomas-Vielma, A. Cervera, B. Levenfeld, A. Varez, "Production of alumina parts by powder injection molding with a binder system based on high density polyethylene", *J. Eur. Ceram. Soc.*, **28** (2008) 763–771.
23. J. Janardhana Reddy, N. Ravi, M. Vijayakumar, "A simple model for viscosity of powder injection moulding mixes with binder content above powder critical binder volume concentration", *J. Eur. Ceram. Soc.*, **20** (2000) 2183–2190.
24. W.-C.J. Wei, R.-Y. Wu, S.-J. Ho, "Effects of pressure parameters on alumina made by powder injection moulding", *J. Eur. Ceram. Soc.*, **20** [9] (2000) 1301–1310.
25. W. Liu, J. Wen, Z. Xie, X. Yang, "Powder modification mechanism, effects of binder compositions on the thermal behavior, and the mechanical properties of the ceramic injection molded system", *Ceram. Int.*, **44** (2018) 5646–5651.
26. M.R.L. Estarki, F.A. Vellashani, F. Moinifard, M. Milani, A. Kumar, M.R. Ghazi, M. Sardarian, "Investigations of selected mechanical, wear properties and transparency of alumina obtained by combined PIM and SPS techniques", *J. Korean Ceram. Soc.*, **59** (2022) 909–919.
27. M.S.K. Masihi, M.R.L. Estarki, H. Mansouri, H. Jamali, M. Sardarian, G.R. Gordani, "Investigation of nanosized alumina-binder feedstock rheology for ceramics injection molding (CIM) and survey spark plasma sintering of output green body to obtain transparent alumina", *Int. J. Appl. Ceram. Technol.*, **19** (2022) 2500–2513.
28. Standard EN 60672-3, "Ceramic and glass-insulating materials - Part 3: Specifications for individual materials".
29. X. Teng, H. Liu, C. Huang, "Effect of Al_2O_3 particle size on the mechanical properties of alumina-based ceramics", *Mater. Sci. Eng. A*, **452-453** (2007) 545–551.
30. H. Tomaszewski, M. Boniecki, H. Weglarz, "Effect of grain size on R-curve behaviour of alumina ceramics", *J. Eur. Ceram. Soc.*, **20** (2000) 2569–2574.
31. A. Krell, "A new look at grain size and load effects in the hardness of ceramics", *Mater. Sci. Eng. A*, **245** (1998) 277–284.
32. A. Krell, P. Blank, "Grain size dependence of hardness in dense submicrometer alumina", *J. Am. Ceram. Soc.*, **78** [4] (1995) 1118–1120.
33. D.-H. Riu, Y.-M. Kong, H.-E. Kim, "Effect of Cr_2O_3 addition on microstructural evolution and mechanical properties of Al_2O_3", *J. Eur. Ceram. Soc.*, **20** (2000) 1475–1481.
34. L. Xu, Z. Xie, L. Gao, X. Wang, F. Lian, T. Liu, W. Li, "Synthesis, evaluation and characterization of alumina ceramics with elongated grains", *Ceram. Int.*, **31** (2005) 953–958.
35. D. Kuscer, I. Bantan, M. Hrovat, B. Malič, "The microstructure, coefficient of thermal expansion and flexural strength of cordierite ceramics prepared from alumina with different particle sizes", *J. Eur. Ceram. Soc.*, **37** [2] (2017) 739–746.